plasma

MDPI

Article

Modeling Streamer Discharge in Air Using Implicit and Explicit Finite Difference Methods with Flux Correction

Hasupama Jayasinghe [1,*], Liliana Arevalo [1,2], Richard Morrow [3] and Vernon Cooray [1]

[1] Department of Electrical Engineering, Division of Electricity, Uppsala University, Box 65, 751 03 Uppsala, Sweden; liliana.arevalo@hitachienergy.com (L.A.); vernon.cooray@angstrom.uu.se (V.C.)
[2] HVDC R&D Department, Hitachi Energy Sweden AB, 722 12 Västerås, Sweden
[3] Department of Applied Physics, Sydney University, Sydney, NSW 2006, Australia; richard.morrow@sydney.edu.au
* Correspondence: hasupama.jayasinghe@angstrom.uu.se

Abstract: Implementing a computationally efficient numerical model for a single streamer discharge is essential to understand the complex processes such as lightning initiation and electrical discharges in high voltage systems. In this paper, we present a streamer discharge simulation in air, by solving one-dimensional (1D) drift diffusion reaction (DDR) equations for charged species with the disc approximation for electric field. A recently developed fourth-order space and time-centered implicit finite difference method (FDM) with a flux-corrected transport (FCT) method is applied to solve the DDR equations, followed by a comparative simulation using the well-established explicit FDM with FCT. The results demonstrate good agreement between implicit and explicit FDMs, verifying their reliability for streamer modeling. The total electrons, total charge, streamer position, and hence the streamer bridging time obtained using the FDMs with FCT agree with the same streamer computed in the literature using different numerical methods and dimensions. The electric field is obtained with good accuracy due to the inclusion of image charges representing the electrodes in the disc method. This accuracy can be further improved by introducing more image charges. Both implicit and explicit FDMs effectively capture the key streamer behavior, including the variations in charged particle densities and electric field. However, the implicit FDM is computationally more efficient.

Keywords: implicit finite difference; explicit finite difference; flux correction; image charges; disc method; streamer discharge

check for updates

Academic Editors: Andrey Starikovskiy and Bruno Caillier

Received: 9 April 2025
Revised: 20 May 2025
Accepted: 24 May 2025
Published: 29 May 2025

Citation: Jayasinghe, H.; Arevalo, L.; Morrow, R.; Cooray, V. Modeling Streamer Discharge in Air Using Implicit and Explicit Finite Difference Methods with Flux Correction. *Plasma* **2025**, *8*, 21. https://doi.org/10.3390/plasma8020021

Copyright: © 2025 by the authors. Licensee MDPI, Basel, Switzerland. This article is an open access article distributed under the terms and conditions of the Creative Commons Attribution (CC BY) license (https://creativecommons.org/licenses/by/4.0/).

1. Introduction

Streamer discharge in air plays a significant role in the initial stages in lightning discharges occurring within clouds or between clouds and the ground. The actual phenomenon observed in the initiation of lightning is that the number of streamers develop from a high electric field region and propagate as a bunch of narrow channels while exhibiting branching [1–3]. When the field maintained by that burst of streamers is high enough, it heats the air and converts to a leader discharge [4–7]. Also, the streamers are important in the formation of electrical discharges under high-voltage conditions in power transmission systems. Streamers form during the high-voltage equipment operation when the local electric field exceeds the ionization threshold, leading to rapid electron avalanches and the development of ionized channels that can initiate partial discharges or electrical breakdown [8–10]. Therefore, analysis of a single streamer discharge from a plasma physics perspective aids in comprehending the behavior of electrical discharges and the role of

factors like temperature, humidity, and pressure on the initiation process of the lightning discharge and on operation in high-voltage power networks.

However, the modeling of even a single streamer is very complex due to its multi-scale nature [11] and extending those models to simulate multiple streamers and their interactions [12], and long-distance streamer propagation across different environmental conditions [9], further amplifies the computational challenges. Hence, it is required to develop a numerical model for a single streamer that is accurate and simultaneously lessens computational demands, while capturing the core physics of streamer discharge.

A streamer model is usually a set of partial differential equations that detail the movement of charged particles, linked with Poisson's equation to account for the electric potential within the discharge area. In the initial phase, pioneering viable streamer models are developed in [13,14]. Subsequently, the modeling approach is improved by solving drift diffusion reaction (DDR) equations for charged particles in 1D, coupled with the Poisson equation in 2D axisymmetric domain [15,16]. This approach is commonly referred to as the 1.5D streamer models [16,17]. To closely mirror the actual particle behavior in a single streamer discharge, the fluid, particle, and hybrid models in 2D or 3D were developed utilizing the finite element method (FEM), finite volume method (FVM) and particle-in-cell (PIC) method, etc. [12,18,19]. This means those higher-dimensional streamer models avoid the self-inconsistency of streamer radius within the 1.5D models even though they necessitate a higher computational footprint.

By incorporating elements of both 1D and 2D or 3D streamer simulations, 1.5D models can effectively simulate the longitudinal development of streamers along with an averaged or simplified representation of radial expansion. This makes them particularly useful for studies wherein a full higher-dimensional model could be computationally prohibitive, yet a simple 1D model could fail to capture critical phenomena. Aleksandrov and Bazelyan found inspiration in the 1.5D model's capacity to simulate streamers based on the finite difference method (FDM) to a greater length than what is possible with simulations of higher dimensions [20]. Similarly, Morrow [15] applies the FDM in combination with flux-corrected transport (FCT) for an adapted computational mesh with time to model a streamer discharge across a 50 mm air gap. This study is extended to a microsecond scale. Using a similar numerical approach, streamer propagation is successfully simulated across a 50 cm of point- plane air gap [21], whereas most of the higher-dimensional models are limited to shorter gap lengths and less time. This study on tens of centimeters long streamer propagation is able to explain the significant details in lightning [9].

The concept of 1.5D streamer models is popular with not only FDM but also other numerical methods such as FVM, FEM, etc. The latest research using a 1.5D FVM streamer model allows for accurate tracking of streamer propagation, bridging, and current flow phases, providing qualitative agreement with experimental current waveforms [22]. By employing the FVM with a moving method to solve DDR equations in 1D, and Poisson equation in 2D, a negative streamer discharge in pure nitrogen gas is successfully simulated [23]. Another study on 1.5D streamer simulation in nitrogen has been conducted recently using a derivative method of the FEM [24]. The short gap breakdown is analyzed using a streamer discharge in the same dimensionality employing both FEM and FDM with flux correction [25].

To elucidate the impact of pressure and humidity on streamer behavior, a 1.5D FDM with FCT model has been employed to simulate the dynamics of streamer propagation which are consistent with the experimental findings [26]. Using explicit FDM with FCT for 1D DDR equations and SOR method for 2D electric field, the negative corona is simulated in a 30 mm rod-plane air gap. This study is capable of estimating the density of charged particles successfully by varying the air pressure and applied voltages [27]. Other examples

of showing the potential of the same 1.5D numerical approach are that the influence from temperature, density, and moisture on long streamer discharge in air is presented in [28,29].

In many types of gas discharges, including streamer discharges, electrons predominantly exhibit drift-dominant nature, leading to numerical challenges such as oscillations and negative values in particle densities, particularly near steep gradients in higher-order schemes of the FDM. Moreover, lower-order schemes of the FDM such as donor cell or Lax–Friedrichs, or higher-order schemes with a zero-order diffusion, exhibit inherent diffusivity in gas discharge simulations [30]. Since both of these issues can be effectively addressed using the FCT technique, FDM has to be implemented together with FCT. To the best of the author's knowledge, FDM-based simulation on gas discharges solves DDR equations explicitly and it has already shown the capability of implementing streamer discharges. Explicit FDM is conditionally stable in terms of time step. However, implicit FDM is more stable even with larger time steps. In [31], implicit FDM with FCT is introduced, although it did not include the diffusion of charged particles in DDR equations. As an improvement of this work, including the implicit diffusion, implicit FDM with FCT has been introduced by Morrow recently [32].

This paper presents the numerical applicability of implicit FDM with FCT including the implicit diffusion on 1.5D streamer simulation in air. The implicit FDM with FCT has fourth-order accuracy which is a higher level of accuracy for charged particle densities compared to most of the streamer discharge simulations available in the literature. Furthermore, in this work, the electric field is obtained using the disc approximation and the accuracy of the electric field is improved by introducing an extended image charge effect to account for the presence of the electrodes. Also, the presented 1.5D streamer model is suitable for achieving results within less computational time. Therefore, the objective of this work is achieved by choosing the suitable dimensionality with an accurate method of calculating both the particle densities and electric field for the streamer discharge model. The streamer computed using the implicit FDM is compared with the streamer simulated using the explicit FDM with FCT in terms of electric field and electron density during both inception and propagation stages. In the streamer calculation, the fixed and adaptive meshes are considered with both the FDMs with FCT. A comparison is made based on the data extracted from 2D models available in the literature to understand the impact of dimensionality and the assumptions of numerical methods on streamer parameters.

This paper is organized as follows: Sections 1 and 2 consist of the introduction and methodology of the streamer modeling. In Section 3, the simulation results are discussed including two different streamer cases, the computational time for the FDM with FCT approaches, the accuracy of electric field, and the comparison of the magnitude of maximum electric field, total electrons, total charge, and streamer positioning in the air gap with 2D streamers documented in the literature. Finally, the concluding remarks are presented in Section 4.

2. Streamer Model

The inception and propagation of a positive streamer discharge in dry air (80% of nitrogen and 20% of oxygen in air) are simulated by obtaining the charged particle evolution with the electric field numerically under the standard pressure and temperature conditions. In this study, it is assumed that only electrons and positive ions contribute to the computation of the streamer. Negative ions are not included in the simulation because their formation in air at standard atmospheric conditions is negligible within the maximum streamer propagation time in this work, which is 20 ns [33–35]. The mobility and diffusivity of the positive ions are neglected as the simulations are running within the nanoseconds scale.

The DDR equations for the electrons and positive ions in an electric field are

$$\frac{\partial N_e}{\partial t} - \nabla \cdot (N_e \mu_e \boldsymbol{E} + D_e \nabla N_e) = S_{ph} + \alpha \mu_e |\boldsymbol{E}| N_e - \eta \mu_e |\boldsymbol{E}| N_e \quad (1)$$

$$\frac{\partial N_p}{\partial t} = S_{ph} + \alpha \mu_e |\boldsymbol{E}| N_e - \eta \mu_e |\boldsymbol{E}| N_e, \quad (2)$$

where N_e and N_p are densities of electrons and positive ions, respectively, in m^{-3} and $\boldsymbol{E}$ is the electric field in $\mathrm{V\,m}^{-1}$. t, μ_e and D_e are time in s, the electron mobility in $\mathrm{m}^2\,\mathrm{V}^{-1}\,\mathrm{s}^{-1}$ and the diffusion coefficient of electrons in $\mathrm{m}^2\,\mathrm{s}^{-1}$, respectively. S_{ph} is a source term accounting for non-local photoionization in $\mathrm{m}^{-3}\mathrm{s}^{-1}$. α, η are the ionization coefficient and attachment coefficient in m^{-1}, respectively. One can refer to [18] for the expressions of μ_e, D_e, α, and η in terms of electric field. The purpose of selecting these expressions is to facilitate a comparison between the present study and the literature [18].

The electric field is determined using the disc method [36]. In the disc method, when the radius of the streamer discharge is finite, the discharge channel is divided into discs (elements) of charges as in Figure 1. Furthermore, it is necessary to include the image charges of the disc charges which take into account the presence of conduction boundaries of the electrodes.

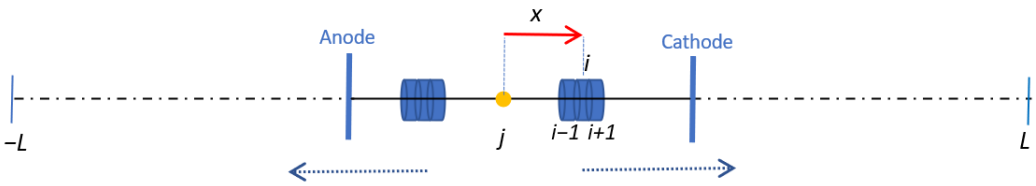


Figure 1. Illustration of the domain for applying the disc method. Full computational domain is in between $-L$ and L. The disc charges are located in between the anode and the cathode (air gap) along the symmetrical axis. The image charges of those disc charges are located outside of the air gap (from $-L$ to anode and from cathode to L).

Then, the electric field at a point along the streamer axis can be calculated as a summation of Laplacian field due to applied voltages, the electric field due to disc charges within the gap, and the electric field due to the image charges of the disc charges. This is represented by Equation (3)

$$\boldsymbol{E}_j = \boldsymbol{E}_{L,j} + \boldsymbol{E}_{c,j}, \quad (3)$$

where $\boldsymbol{E}_j$, $\boldsymbol{E}_{L,j}$, and $\boldsymbol{E}_{c,j}$ are the electric field at the point j on the symmetrical axis of the streamer channel, Laplacian field at the point j, and electric field due to both disc charges and their image charges at the point j in $\mathrm{V\,m}^{-1}$. The Laplacian electric field is given by Equation (4) and solved using the applied voltages on electrodes as the boundary conditions.

$$\begin{aligned} \epsilon \nabla \cdot \phi &= 0\,, \\ \boldsymbol{E}_{L,j} &= -\nabla \phi, \end{aligned} \quad (4)$$

Here, ϵ and ϕ are the permittivity of free space in $\mathrm{F\,m}^{-1}$ and the electrical potential in V, respectively. The electric field due to both the disc charges and image charges is calculated using

$$\boldsymbol{E}_{c,j} = \frac{1}{2\epsilon} \int_{-L}^{L} \rho(i) \left(\frac{x}{|x|} - \frac{x}{\sqrt{x^2 + R^2}} \right) dx, \quad (5)$$

where $\rho(i)$, L, x and R are the charge density of i^{th} disc in the streamer channel in cm^{-3}, the distance including disc charges and image charges in each side of electrode in m, the distance from the point j to i^{th} disc in m, and the radius of the discharge channel in m,

respectively. Thus, to apply the disc method, it is assumed that the radius of the ionized channel is finite and the charges are distributed uniformly along the radial direction in each disc in the discharge channel. In this study, the radius of the streamer channel is assumed in the range of 320–340 µm to ensure to have the closely aligned initial electric field to the published results in [18]. Therefore, a meaningful comparison with the literature in Section 3.5 can be facilitated.

The accuracy of the electric field is evaluated with the number of sets of image charges included in the simulations. The results in Section 3 are presented by utilizing three sets of image charges on each side of the electrodes, which gives enough accuracy for the electric field in the study.

The computational domain is shown in Figure 2 with a 2D axisymmetric view. It consists of a 1.25 cm long parallel-plane air gap. Thus, L in Figure 1 and Equation (5) is 3.75 cm for three sets of image charges on each side of the electrodes. The high voltage (18.75 kV) is applied to the top anode and the bottom cathode is grounded. Due to these applied voltages, 1.5 MV m^{-1} of the downward uniform initial electric field (E_{init} in Figure 2) is generated within the air gap. Since the initial electric field is not enough to have the effective ionization in the domain, as seen in Figure 2, a Gaussian seed of positive ions at 0.01 m above from the cathode is placed to enhance the initial background field above the breakdown electric field of air. The initial seed of positive ions is described by Equation (6).

$$N_p = 10^{13} + 5 \times 10^{18} \exp\left(-\frac{(z - z_0)^2}{\sigma^2}\right) \mathrm{m}^{-3}, \tag{6}$$

where z is axial coordinates. $z_0 = 0.01$ m and $\sigma = 0.0004$ m [18].

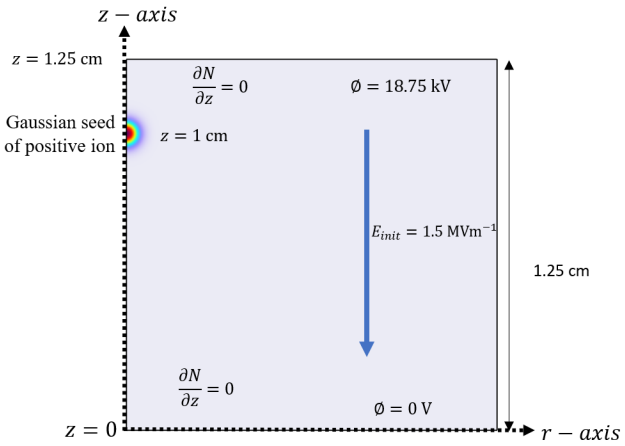


Figure 2. A 2D axisymmetric representation of 1.25 cm long air gap with a parallel-plane electrode configuration based on [37]. The initial Gaussian seed of the positive ions is located at $z = 1$ cm. N and ϕ are electrons or positive ion densities and electrical potential, respectively.

For this study, DDR equations for electrons and positive ions are solved along the symmetrical axis in Figure 1, which means that charged particle densities are obtained in 1D. For both the electrons and positive ions, all boundaries have homogeneous Neumann boundary conditions. Equations (1) and (2) are solved using the fourth-order space and time-centered implicit FDM with FCT including second-order differencing of the diffusion term [32] with the Boris flux correction method [38]. For gas discharge calculations, this approach is much more suitable due to the higher accuracy and stability of the solution. The reason behind choosing the Boris flux limiter instead of the Zalesak flux limiter is that the Boris flux limiter requires less computational time even though both limiters yield identical outcomes in this computation [30]. The explicit FDM used in this study is described in [39], and it is also implemented together with the Boris flux limiter. Using the second-order

Runge Kutta method, the source terms are evaluated in DDR equations of electrons and positive ions [40].

The streamer discharge is modeled under two different cases which are stated below. The difference between these two cases are the background ionization levels and and, in only one case, photoinization is taken into account.

1. Case 1: Background ionization is 10^{13} m^{-3} and the photoionization is not considered as a source of electrons and positive ions.
2. Case 2: Background ionization is 10^{9} m^{-3} and the photoionization is considered as a source of electrons and positive ions.

The effect of photoionization is implemented from Equation (7) which is derived based on the experimental work published in [41].

$$S_{ph} = N_D \varphi_{rp} \theta d p \, , \tag{7}$$

Here, θ, d, and p are the solid angle in sr, the thickness of the region where photoionization occurs in cm, and the pressure is in Torr, respectively. N_D represents the number of ion pairs generated in m^{-3}s^{-1}, which is assumed to be equivalent to the electron ionization rate per unit volume. N_D is calculated using the expression $\alpha \mu_e |\boldsymbol{E}| N_e$. For consistency, the coefficients for α and μ_e are adopted from [18], which are the same used for solving Equations (1) and (2). φ_{rp} is the yield of photoionization in sr^{-1} Torr^{-1} cm^{-1} which can be obtained through the empirical data provided in [41]. Unlike the 2D or 3D fluid or particle tracing methods, the FDMs are allowed to use direct photoionization values in Equations (1) and (2). This is beneficial in maximizing the computational performance, which is important in the simulations at the microscopical level.

For the computational analysis, two mesh varieties are utilized. First, to facilitate both streamer cases with both FDMs with FCT, the uniform meshes are selected. For case 1 and 2, the mesh element sizes of the uniform meshes are 5 µm and 4 µm, respectively. These mesh sizes represent the largest element sizes that ensure the numerical stability while maintaining the sufficient spatial resolution for the accurate representation of the streamer dynamics in the simulations. Secondly, an adaptive non-uniform mesh with time is used for case 1 only, to check the capability of handling adaptive meshes by the implicit and explicit FDM with FCT. In the adaptive mesh, the head of the streamer is always located within a region of uniformly distributed finest mesh elements. In explicit FDM with FCT, the size of the finest mesh elements around streamer front is 1 µm, yet the implicit FDM with FCT can handle 4 µm mesh elements around the streamer head. A similar construction of an adaptive mesh is detailed in [42].

The time step of the implicit FDM with FCT is defined under the following two conditions:

1. Courant–Friedrichs–Lewy (CFL) condition.
2. Change in magnitude of the electric field in a time step should be lower than 10%.

The implicit fourth-order time and space-centered algorithm does not provide strictly positive results on its own; thus, it must be coupled with upwind differencing for the convective term in lower-order scheme and a flux-corrector in order to create an FCT algorithm that gives strictly positive results [32]. Since the upwind difference scheme is subject to the CFL condition, then the entire algorithm must obey the CFL condition.

The CFL condition is associated with the DDR behavior of the charged particles and does not consider the variations in the electric field resulting from the movement of charges. Therefore, when particle densities are high, the transport algorithm may allow for a quantity of charge movement within one time step that is sufficient to invert the driving field. The second condition is implemented to stop huge changes and hence reverse the driving field due to the movement of charges. Otherwise, the numerical oscillations can develop step by

step [43]. This confirms that the electric field obtained below does not have major variations with a time step.

In explicit FDM with FCT approach, the diffusion term is calculated explicitly. Hence, there is a condition to be concerned with in addition to the above two conditions. It is the Von Neumann time step condition, which is related to the explicit diffusion of the algorithm [44]. However, there is no time step restriction in the implicit FDM with FCT method due to the implicit diffusion as it integrates into the method itself to have a vigorous computational procedure [32].

3. Results and Discussion

In this section, initially the results are presented for the variations in electric field and electron density of both the streamer cases 1 and 2, utilizing both the implicit and explicit FDM with FCT. Those results are depicted in Figures 2–7, where, in each figure, the cathode and anode are positioned at distances of 0 cm and 1.25 cm, respectively. Hence, the positive streamer is always propagating from right to left. Secondly, the computational efficiency in terms of computational time consumed by each streamer model is examined. Thirdly, the relation between the accuracy of the electric field in the streamer modeling and the number of sets of image charges are evaluated. Finally, a comparison is provided on the streamer parameters including the maximum electric field, total number of electrons, total charge, and the streamer position obtained from implicit, explicit FDM with FCT, and 2D fluids models in [18].

3.1. Case 1: Electric Field and Electron Density Using Implicit and Explicit FDM with FCT

The streamer discharge in case 1 initiates and advances in a higher background ionization level than case 2 and without the source of photoionization. The electric field evolution of the streamer across the gap distance along the z-axis at different time instances is shown in Figure 3a,b, which are generated utilizing the implicit and explicit FDM with FCT, respectively. In the same figures, the numerical influence on the fixed uniform and adaptive non-uniform meshes from both algorithms are also illustrated for the electric field evolution during streamer propagation. Here, the continuous lines and dashed lines show the electric field variation on fixed and adaptive meshes, respectively. The electron density variation along the symmetrical axis during the streamer propagation is shown in Figure 4a for the implicit FDM and Figure 4b for the explicit FDM.

To closely evaluate the differences in the electric field variation obtained using both FDMs and two types of meshes, the peak electric field values at 2 ns and 16 ns are considered. According to Figure 3a,b, at 2 ns the peak electric field occurs around at 0.9 cm in both mesh types using both FDM approaches. However, in the implicit FDM, this peak electric field is 0.119 $\mathrm{MVcm^{-1}}$, while the explicit method shows 0.120 $\mathrm{MVcm^{-1}}$ of peak electric field for both mesh types. In Figure 3a at 16 ns, the peak electric fields obtained on the fixed mesh and adaptive mesh using implicit FDM with FCT are approximately 0.175 $\mathrm{MVcm^{-1}}$, which occurs at around 0.19 cm, and 0.178 $\mathrm{MVcm^{-1}}$ occurs at around 0.16 cm, respectively. Figure 3b indicates that both the fixed and adaptive meshes exhibit similar peak electric fields to 0.170 $\mathrm{MVcm^{-1}}$ using the explicit FDM approach at 16 ns, although this peak field happens at around 0.20 cm and 0.21 cm on the z-axis for the fixed and adaptive meshes, respectively. When the same analysis is applied to Figure 4a,b, at 2 ns and 16 ns, the electron densities around the streamer head are $5.45 \times 10^{19}\,\mathrm{m^{-3}}$ and $1.87 \times 10^{20}\,\mathrm{m^{-3}}$, respectively, for the implicit FDM, whereas the explicit method obtains $6.17 \times 10^{19}\,\mathrm{m^{-3}}$ and $1.32 \times 10^{20}\,\mathrm{m^{-3}}$ electron densities for the same time instances, respectively.

As the differences in the electric field and electron density obtained from both the implicit FDM with FCT and explicit FDM with FCT are very slight, the results show

good agreement. Furthermore, it can be noted that both meshes yield very similar results, suggesting that the FDM with FCT can be utilized on adaptive meshes without leading to numerical instabilities. Thus, enabling the use of adaptive meshes makes it possible to extend the application of the FDM with FCT to tenth of centimeters or even meters long gap distances.

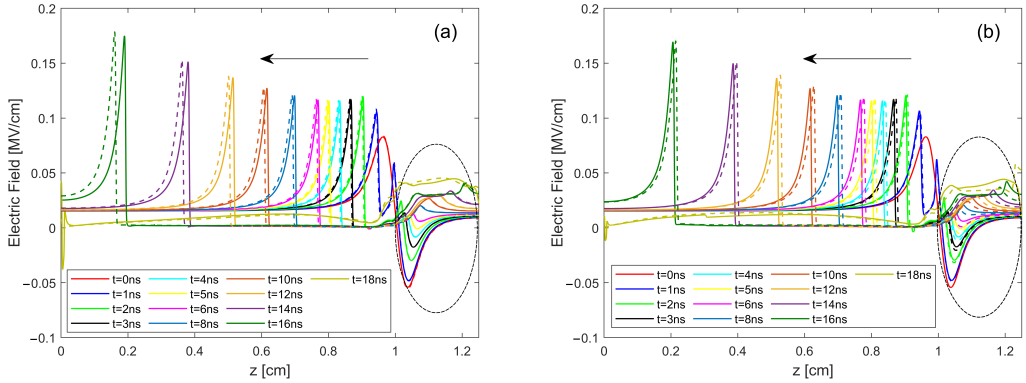


Figure 3. Electric field versus distance along the z- axis during the streamer propagation time using (**a**) implicit FDM with FCT and (**b**) explicit FDM with FCT. The continuous and dashed line represent the values from fixed mesh and adaptive mesh, respectively. The dotted circle marks the area behind the streamer initiation point, where the direction of the electric field changes during the streamer propagation time. The black arrow in each figure shows the direction of the streamer propagation.

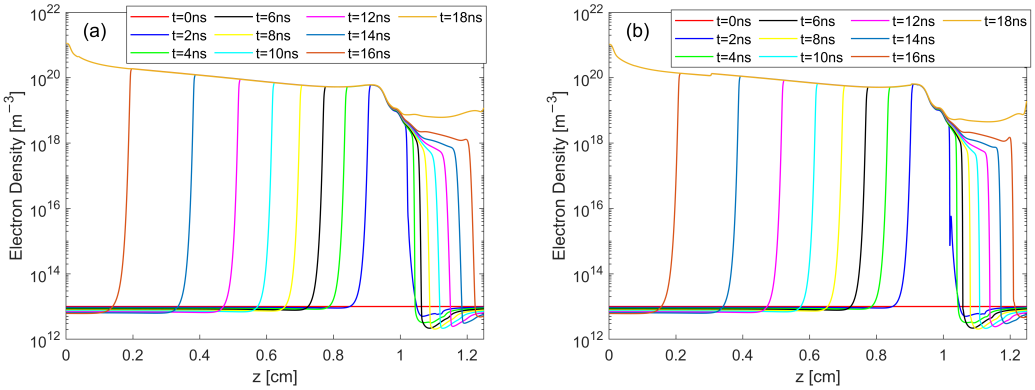


Figure 4. Electron density as a function of z coordinates at different time instances during the streamer advancement using (**a**) implicit FDM with FCT and (**b**) explicit FDM with FCT.

Figure 3a,b are plotted assuming the positive electric field acts in the direction towards the cathode from the anode. According to those two figures, initially, the air gap consists of both the positive and negative directional background electric fields (red color line, $t = 0$ s) due to the positive ion seed which is located near the anode. The negative electric field happens between the anode (at 1.25 cm) and the positive ion seed (at 1 cm), seen inside the dotted ellipse in Figure 3a,b. With this initial field distribution, the streamer formation starts approximately at $z = 1$ cm, where the enhanced positive background electric field occurs initially due to the seed.

During 0–2 ns, a growth of the electric field at the streamer head can be observed in Figure 3a,b. This represents the streamer formation stage, which is the transition from the initial ionization processes to the dynamic growth phase of the streamer. After 2 ns, the electric field at the streamer head tends to reduce until approximately 5 ns. This is the phase of relaxation in the electric field during the streamer advancement. On the other hand, until 5 ns, the initial negative electric field between the initial seed and the anode is still there at a decreasing rate. After around 5 ns, that negative field becomes positive and

the whole air gap consists of a positive electric field. This results in the electric field at the streamer head after 5 ns starting to increase during its propagation towards the cathode.

To clearly understand this transition at around 5 ns, the electric field and the densities of electrons and positive ions at 5 and 8 ns are depicted in Figure 5a and 5b, respectively. Figure 5a shows that, behind the streamer initiation point (1–1.25 cm), there are more positive ions than electrons. Until 5 ns, the area behind the streamer initiation point is positively charged, but that positivity is decreasing with time due to the presence of more electrons in that area. Even though the electrons and positive ions are generated at the same rate according to Equation (1) and (2), this behavior can occur due to the drift and diffusion of electrons, which does not apply in the same way to positive ions.

According to Figure 5b, at 8 ns the electrons are becoming dominant in the region marked with the dotted circle. Due to the presence of higher electron density than positive ions between the anode and the streamer initiation point after 5 ns, the negative electric field becomes positive. This might be the reason to increase the electric field at the head of the streamer after 5 ns since the developing electron cloud in between the anode and the streamer initiation point may cause higher conductivity in the streamer channel and hence more positive ions in the streamer head.

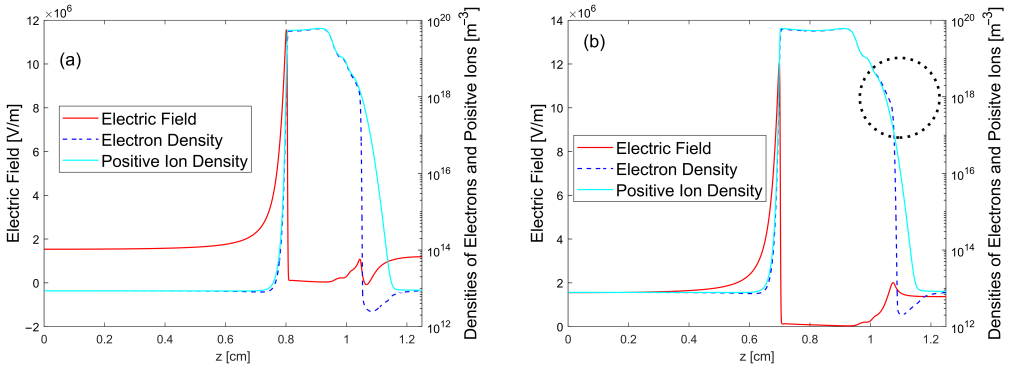


Figure 5. Electric field, electron density, and positive ion density variation at (**a**) 5 ns and (**b**) 8 ns along the *z*-axis. Red, blue dashed, and cyan colors represent the electric field, electron density, and positive ion density, respectively. The dashed circle shows the area behind the streamer initiation point where the electron density becomes more dominant than positive ions.

To verify the electric field during the streamer propagation, the line integral of the electric field along the symmetrical axis in each time step is computed. The values are very close to the applied voltage with a maximum tolerance of 0.14% and 0.13% for the implicit and explicit methods, respectively. This implies that the streamer modeling in this work achieves the electric field values with greater accuracy during streamer propagation. To increase even further, these tolerances through the application of the image charges in the disc method will be detailed in Section 3.4.

Figure 4a,b indicate that the streamer bridges the gap between 16 ns and 18 ns. The electron density grows approximately up to 1×10^{21} m^{-3} in both the FDM approaches at 18 ns around the cathode. In addition, after the streamer bridges the gap, the electric field diminishes with time. This is illustrated in Figure 3a,b at 18 ns.

3.2. Case 2: Electric Field and Electron Density Using Implicit and Explicit FDM with FCT

In case 2, a streamer discharge is studied with the reduced background ionization compared to case 1 and with the impact of the photoionization. The initial background electric field remains analogous to case 1 as the applied voltages and the initial seed are the same. Figure 6a,b illustrate the electric field variations as a function of the gap distance at different times using the implicit and explicit FDM with FCT, respectively, on the fixed mesh.

The electron density variation along the streamer advancing distance during different times is plotted in Figure 7a,b for implicit and explicit FDM with FCT, respectively.

It is clear that both approaches provide similar results for the streamer behavior in terms of the electric field and electron density in case 2. One can clearly see that, in Figure 6a,b, the electric field at the streamer head grows until 3 ns which means that the streamer formation occurs during that time. Then, during 3–5 ns, the electric field at the streamer head decreases, which is the field relaxation period. After 5 ns, with the electric field along the whole gap becoming positive, the electric field at the streamer head starts to increase again until the streamer bridges the air gap. Similar to case 1, this observed electric field variation results from the changes in the distributions of electrons and positive ions densities. The detailed explanation is provided in Section 3.1.

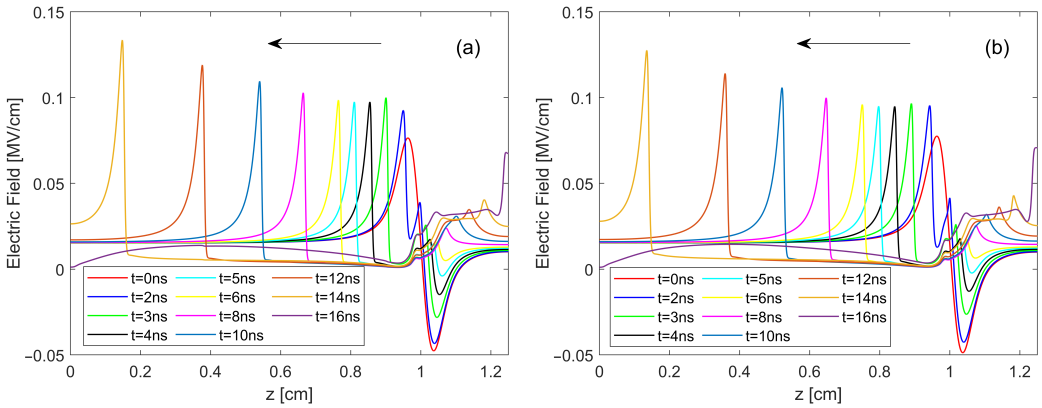


Figure 6. Electric field in case 2 as a function of a distance along z-axis at different time steps (**a**) employing implicit FDM with FCT, (**b**) explicit FDM with FCT.

The electric field along the streamer axis during its advancement is verified in the same way as case 1 using the line integral of the electric field. The error margin is 0.18% and 0.21% of the applied voltage for the implicit and explicit approaches, respectively. Figure 7a,b show that the streamer bridges in between 14 and 16 ns in case 2. With the streamer bridging at the cathode, the electron density reaches approximately 5×10^{20} m^{-3} in both implicit and explicit FDM with FCT approaches. Furthermore, after the streamer bridges, Figure 6a,b show that the electric field is reducing at 16 ns.

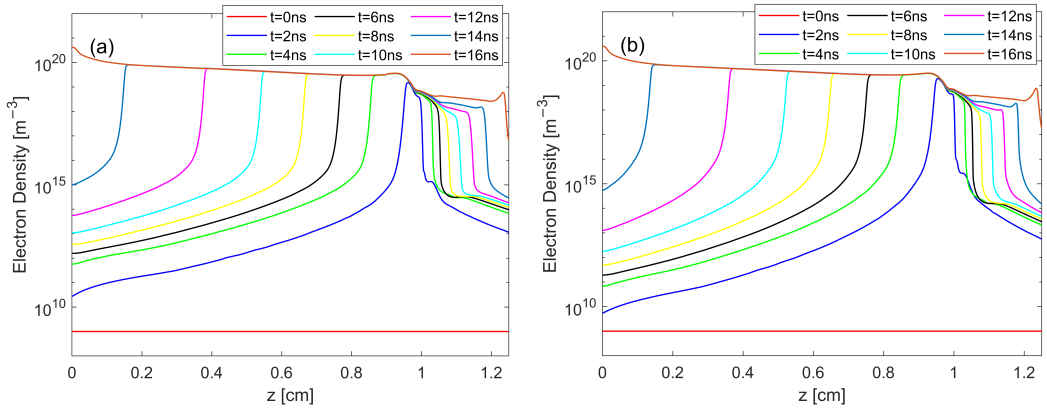


Figure 7. Electron density as a function of a distance along z-axis at different time instances using (**a**) implicit FDM with FCT; (**b**) explicit FDM with FCT.

A positive streamer is propagating with the aid of free electrons in front of its head. To create free electrons and hence to advance the positive streamer discharges, an important contribution is provided by photoionization in air according to [45,46]. By comparing case 1 and 2, the impact of the photoionization on the streamer propagation is analyzed. The

time it takes for the streamer to reach the cathode in case 1 and 2 indicates that the streamer discharge in case 2 is faster than case 1 even though the background ionization level is lower in case 2. If the background ionization is lower, the streamer propagation is slower according to [18,19,47]. This means that, in case 2, the positive streamer is accelerated by the photoionization. This is consistent with the literature [48].

In case 1 and 2, the streamer head reaches approximately 0.75 cm along the z-axis after 6.7 and 6 ns, respectively. Figure 8 shows the effective impact ionization rate per unit volume and the photoionization rate per unit volume of case 2 at 6 ns. In the same figure, the effective impact ionization per unit volume of case 1 is plotted at 6.7 ns. The effective impact ionization rate per unit volume in both cases is calculated as $\alpha\mu_e|\boldsymbol{E}|N_e - \eta\mu_e|\boldsymbol{E}|N_e$. The field-dependent coefficients of α, η, and μ_e are obtained from [18].

When the streamer head is around 0.75 cm, the maximum effective impact ionization rates per unit volume for case 1 and 2 are $6.9 \times 10^{29}\,\mathrm{m^{-3}s^{-1}}$ and $2.4 \times 10^{29}\,\mathrm{m^{-3}s^{-1}}$, respectively. Due to the higher background ionization level in case 1, the effective impact ionization rate per volume is higher than case 2 around the streamer head. The maximum photoionization rate per unit volume of case 2 at 6 ns is $1.9 \times 10^{26}\,\mathrm{m^{-3}s^{-1}}$. Even though the magnitude of the effective impact ionization rates per unit volume of case 1 and 2 are higher than the photoionization rate per unit volume, the photoionization rate per unit volume makes the ionization zone wider around the streamer head. In other words, photoionization extends the ionization region beyond the immediate high field area near the streamer head, enabling a more effective electron avalanche formation and hence a more continuous and efficient streamer propagation mechanism. This may account for the faster propagation of the streamer in case 2 compared to case 1.

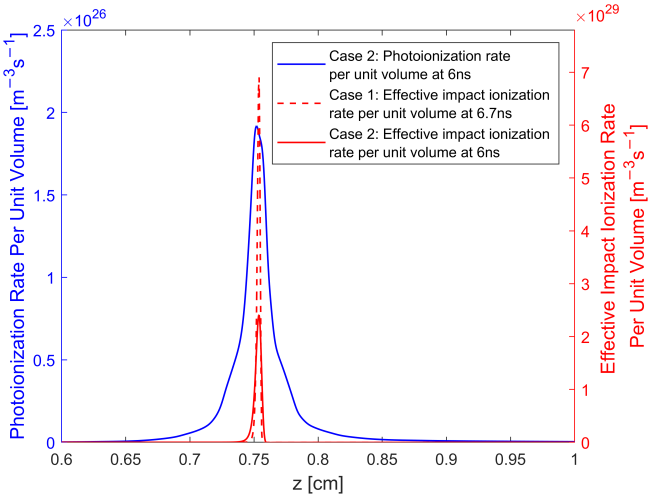


Figure 8. When streamer head is located approximately at 0.75 cm along the z-axis, effective impact ionization rate per unit volume for case 1 is shown at 6.7 ns, along with photoionization rate per unit volume and effective impact ionization rate per unit volume for case 2 at 6 ns. Case 1 is simulated with only effective impact ionization as source terms for electrons and positive ions, while both photoionization and effective impact ionization is considered in case 2. Shown is the 0.6–1 cm segment of the 1.25 cm air gap along the z-axis, selected for detailed visualization through zooming.

3.3. Comparative Analysis of Computational Efficiency of Streamer Calculation Using FDMs with FCT

This analysis is based on the streamer discharge obtained in case 1 and case 2 only on the fixed mesh. The adaptive mesh is used solely to demonstrate the implicit and explicit algorithms' compatibility with different mesh types in Section 3.1, rather than the computational performance. The computational time for each algorithm is discussed. In each streamer case, the difference happens in FDM and the same FCT technique is applied.

Therefore, mainly, the computational time of each simulation is influenced by the size of the time step. Implicit FDM allows for a time step that is twice as long as that the explicit FDM and time step limitation from explicit diffusion has to be concerned in explicit FDM. On the other hand, the implicit FDM spends additional time to compute lower and higher-order fluxes and to calculate implicit time discretizations. In other word, the per-time step computational overhead in implicit FDM is higher compared to explicit FDM.

For case 1 and 2 on the fixed uniform mesh, the computational time is consumed by both FDMs until streamer bridges are stated in Table 1. According to the values in Table 1, in each streamer case, the implicit method takes less computational time in order to produce oscillation-free results while protecting the positivity. This implies that the benefit of employing larger time steps in the implicit method significantly outweighs its higher computational cost per time step, leading to a shorter total computational time compared to the explicit method.

Streamer case 2 exhibits a higher computational time regardless of the FDM employed. This is because the uniform mesh in case 2 is finer than in case 1 (see Section 2) and the inclusion of the calculation of photoionization, despite the time for the streamer to bridge the gap shorter in case 2.

Table 1. Computational time for streamer case 1 and case 2 using both FDMs with FCT.

Streamer Case	Implicit FDM with FCT (mins)	Explicit FDM with FCT (mins)
Case 1	20	90
Case 2	250	380

3.4. Accuracy of the Electric Field

In streamer simulations, achieving high accuracy in computing the electric field is critical, as even slight fluctuations in the electric field can lead to significant changes in particle densities. The electric field in the air gap due to the space charges is determined in this paper using the disc method and, to verify the results in each time step, the line integral of the electric field is calculated as stated above. Generally, the error of the line integral of the electric field is not constant for each time step. In each case using each FDM with FCT, the maximum error which is the maximum difference between the line integral and the applied voltage is obtained while varying the sets of the image charges which represents the effect of the space charges within the air gap on the parallel electrodes in the disc method. Table 2 displays the obtained maximum error margin for both case 1 and 2 using the implicit and explicit FDM with FCT from one to four sets of image charges on each side of the electrodes.

Many of the electric field calculations using the disc method rely on just one set of mirror charges, whereas some use none at all. However, a notable observation from the figures in Table 2 is that the maximum error of the line integral of the electric field along the streamer channel can be minimized by extending the sets of mirror charges behind the electrodes. This implies the importance of implementing the effect from image charges in the disc method to calculate the electric field due to space charges. Furthermore, this maximum error usually happens in each streamer case, when the streamer is about to bridge the air gap.

Table 2. Maximum error of the electric field variation in case 1 and 2 under both FDMs with FCT with the expansion of image charges.

Number of Sets of Image Charges in Each Side of Electrode	Maximum Error (%) of Case 1		Maximum Error (%) of Case 2	
	Implicit	Explicit	Implicit	Explicit
1	0.64	0.66	0.75	0.69
2	0.37	0.4	0.55	0.60
3	0.14	0.13	0.18	0.21
4	0.087	0.084	0.054	0.077

3.5. Comparative Analysis of FDM with FCT Streamer Results and Prior Studies

Cases 1 and 2 in Section 2 are also analyzed in [18] using different 2D fluid models. Therefore, this section presents a comparison of key streamer characteristics such as the maximum electric field, total number of electrons, total charge in the domain, and streamer position in the air gap between the streamer simulations obtained in this paper and the results published in [18] for the streamer calculations using the 2D models. However, a comprehensive comparison is limited in this study, since the difference in model structure of streamer discharge (1.5D vs. 2D) and the differing model assumptions such as the use of a constant streamer radius in this numerical simulation limit which features can be directly compared. Additionally, the limitations in the available published data make it difficult to conduct a thorough analysis for the streamer parameter sensitivities and quantitative error estimation.

First, the magnitude of electric field and electron density values are compared between case 1 and case 2 using Figures 3, 4, 6 and 7. It can be observed that both the magnitude of electric field and electron density of case 2 during the streamer propagation are lower than in case 1, which is consistent with [18]. Then, the variation of the maximum electric field over $l(t)$ for case 1 and case 2 are plotted in Figure 9a and 9b, respectively. Here, the maximum electric field during both streamer inception and propagation occurs at the streamer tip. $l(t)$ is calculated using Equation (8).

$$l(t) = L_g - z_m(t)\,, \tag{8}$$

where L_g is the gap length between the anode and cathode in cm (1.25 cm in this work). $z_m(t)$ is the z-coordinate corresponding to the maximum electric field in cm, which changes with time t.

Figure 9a,b also include the results from different 2D streamer models obtained from [18] for the comparison. In both cases, when $l(t)$ is approximately 0.35 cm, the streamer computed using FDMs with FCT is initiated with a lower maximum electric field compared to the 2D streamers. Specifically, the maximum electric field approximately at 0.35 cm, calculated using the FDMs with FCT, is 25% and 7% lower in streamer case 1 and case 2, respectively, than the lowest maximum field observed among the different 2D models.

After the streamer initiation in each case using FDM approaches, the maximum electric field initially decreases slightly before increasing again during the streamer advancement. The underlying reason for this variation is explained in Sections 3.1 and 3.2. This trend of the slight decrement in maximum electric field after the streamer initiation can be seen in the results obtained in some 2D groups; for instance, the 2D group 1 in Figure 9a and the 2D group 2 in Figure 9b.

Furthermore, the maximum electric field obtained using FDMs with FCT nearly from $l(t) = 0.35$ cm to $l(t) = 0.8$ cm in both streamer cases are lower than 2D results. In [18], the streamer radius variation in 2D simulation for only the streamer case 2 is provided. The initial radius is around 400 µm and it suddenly reduces to approximately 250 µm (within around 1 ns during the streamer inception) and gradually increases up to 450 µm by the time the streamer bridges the air gap. It can be noted that, once $l(t)$is around at 0.8 cm in case 2 in the 2D simulation, the radius closely matches the radius assumed in this paper which is in the range of 320–340 µm. At this instance ($l(t)$is around at 0.8 cm in Figure 9b), the close agreement between maximum electric field obtained from both FDMs with FCT approaches and 2D simulation occurs for the streamer in case 2. This suggests that the maximum electric field of the streamer from FDMs with FCT becomes closer to the 2D results when the radial extent of the streamer channel in 2D simulations aligns with the streamer radius assumption in 1.5D.

When the streamer is close to the cathode in both streamer cases ($l(t)$ is around 0.95–1.1 cm in Figure 9a,b), the maximum electric field increases, exceeding the values observed in the 2D results. For case 2, this can be explained again using the streamer radius in 2D results. When $l(t)$ is approximately between 0.95 and 1.1 cm, the streamer radius of the reported 2D modeling is higher than the radius assumed in this work. Also, in case 2, the differences on the maximum electric field throughout the streamer inception and propagation may arise from the variations in how photoionization is numerically treated between the current work and in [18].

Although we could not provide a detailed explanation for the differences in the maximum electric field in case 1 by directly analyzing the streamer radius variations (due to the absence of radius data in [18]), it is reasonable to conclude that the streamer radius assumed in this study influences these differences in the maximum electric field in the streamer discharge compared to 2D results. This point is further confirmed in [49]. More broadly, the differences observed in the maximum electric field in both streamer cases can be attributable to the assumption employed in the disc method, which is that the charge distribution along the streamer channel is uniform to calculate the electric field due to the space charges.

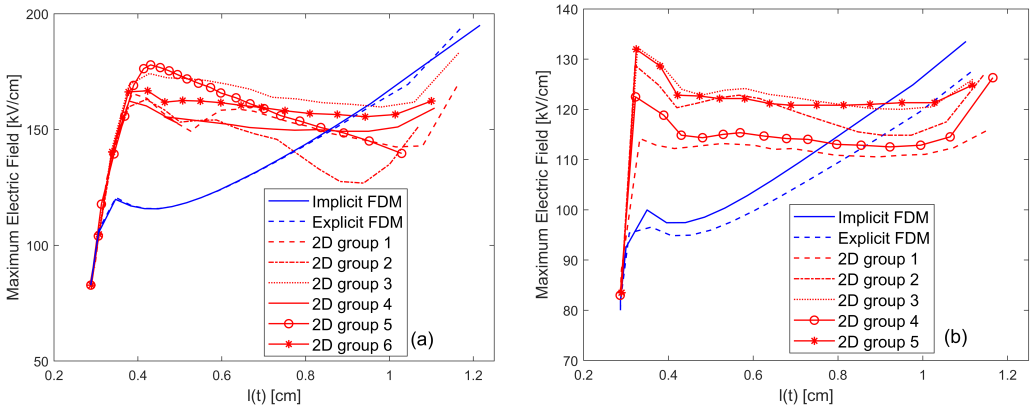


Figure 9. Maximum electric field variation during the streamer propagation for (**a**) case 1 and (**b**) case 2 using the implicit FDM with FCT (blue continuous line), explicit FDM with FCT (blue dashed line), and 2D fluid models (different styled red color lines) in [18].

The number of total electrons variation over $l(t)$ is shown in Figure 10a,b for case 1 and 2, respectively. The total number of electrons is calculated by multiplying the electron density along the z-axis with the cross-sectional area of the streamer and integrating it along the z-axis. A clear agreement is observed in the total electrons for both streamer cases computed using FDM approaches compared to the available 2D results. This implies that

assumption of the finite streamer radius in this study does not have an effect on the total electrons in the computational domain, which is pointed out in [22] also for a 1.5D model based on FVM. Furthermore, the total charge in both cases during the streamer inception and propagation should be conserved as the source terms for electrons and positive ions, which are equal in Equations (1) and (2). The initial total charge due to the positive seed is equal in both streamer cases and it is 0.220 nC for the streamer calculation using FDMs with FCT. It is noticeable that this initial charge is conserved throughout the simulation time, while the conserved total charge in 2D streamers is 0.285 nC. This reveals that the total charge in the presented work is nearly in agreement with 2D results.

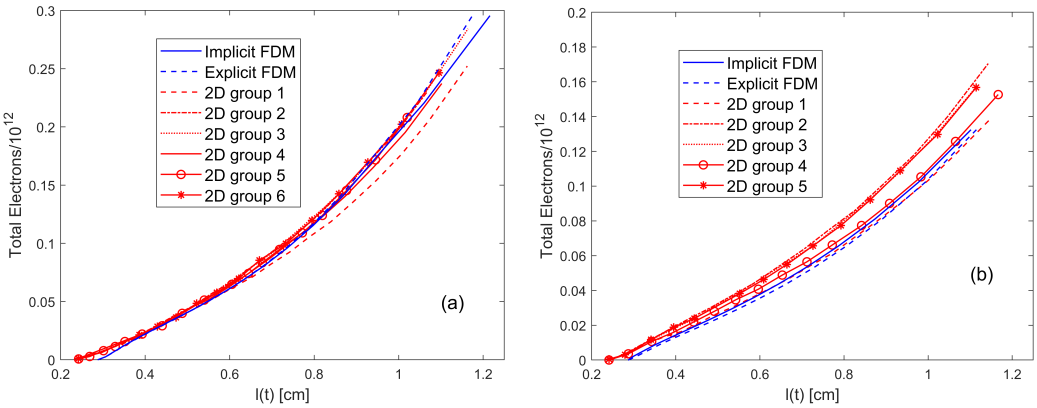


Figure 10. Total electrons variation across $l(t)$ for (**a**) case 1 and (**b**) case 2 using the implicit FDM with FCT (blue continuous line), explicit FDM with FCT(blue dashed line), and 2D fluid models (different styled red color lines) in [18].

With the purpose of identifying the difference between models on the streamer head positioning, [18] introduces the concept of adjusted streamer length. The adjusted streamer length is calculated as

$$L_{adj}(t) = l(t) - v \times t' \,, \tag{9}$$

where L_{adj} and t' are adjusted streamer length in cm and time in ns, respectively. v is the velocity which exhibits the values of 0.05 cm ns^{-1} for case 1 and 0.06 cm ns^{-1} for case 2 [18]. Figure 11a,b show the temporal adjusted streamer length for case 1 and case 2, respectively. Both figures include the results for adjusted streamer length during the propagation time obtained using FDMs with FCT, as presented in this paper, and the results extracted from different 2D streamer models in [18].

In Figure 11a, 2D streamer models have considerable deviations from each other over time and their air gap bridging time also varies approximately between 16 and 18 ns, which is consistent with the bridging time obtained from both FDM models discussed in this paper. According to the same figure, the adjusted streamer length from the steamer models based on the implicit and explicit FDMs are mostly varying within the values obtained in 2D fluid models for case 1. If a closer look at the details is taken in Figure 11a, it can be observed that the adjusted streamer length, acquired using the implicit FDM and explicit FDM, shows the maximum deviation from the slowest 2D streamer around at 10 ns, with the rough deviation values of 0.01 cm.

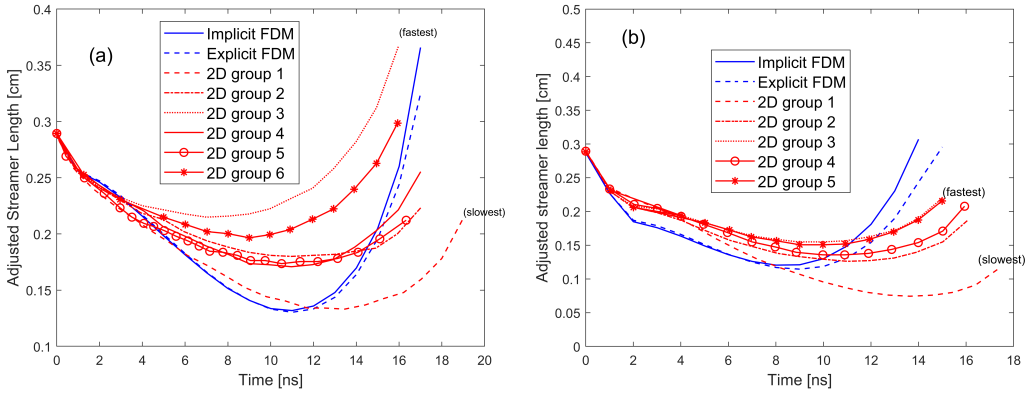


Figure 11. Adjusted streamer length versus propagation time for (**a**) case 1 and (**b**) case 2 using the implicit FDM with FCT (blue continuous line), explicit FDM with FCT (blue dashed line), and 2D fluid models (different styled red color lines) in [18].

In case 2, the adjusted streamer length values computed using FDMs with FCT are lower than the 2D streamers during an approximately 1–8 ns interval. Within this period, the maximum difference between 2D streamers and the results gathered from both FDMs with FCT is approximately 0.02 cm around at 4 ns. As discussed earlier, this slower propagation of the streamer obtained using FDMs with FCT may be attributed to the lower maximum electric field than in 2D steamers observed up to approximately 0.8 cm in Figure 9a,b.

After around 12 ns, streamers calculated using FDMs with FCT have faster propagation until it bridges the gap. Adjusted streamer length obtained from implicit FDM with FCT and fastest 2D streamer has the maximum difference of 0.1 cm at around 14 ns. The adjusted streamer length obtained from explicit FDM with FCT is 0.075 cm higher than the fastest 2D streamer at 15 ns, which is the maximum difference. This faster propagation of the streamers computed using FDMs with FCT in case 1 and 2 may be linked to the higher maximum electric field after approximately around 1 cm, as discussed above and shown in Figure 9a,b.

In [18], it is claimed that the maximum difference between the slowest and the fastest 2D streamers in case 2 is approximately 0.2 cm at around 15 ns. However, it is clear that all the maximum deviations from 2D results to the results obtained from FDMs with FCT are lower than 0.2 cm, and hence the adjusted streamer length acquired from FDMs with FCT aligns closely with 2D outcomes. Moreover, in Figure 11b, the variation between the bridging time of 2D streamers is around 15–17 ns and the results in this work fall closely within that range.

A comparison between 1.5D models with FDM approaches and 2D streamer simulations shows that, while the maximum electric field exhibits variations, likely due to the differences in streamer radius, the total number of electrons, total charge in the domain, and overall streamer positioning in the air gap over time remain consistent. Therefore, in high voltage and lightning discharge modeling wherein an estimation of total electrons or total charge in the system or the temporal variation in the streamer position are required, 1.5D streamer modeling based on FDMs with FCT can provide a reasonable approximation.

4. Conclusions

This paper presents the streamer discharge simulation in air under standard atmospheric pressure and temperature, employing both the fourth-order accurate, implicit FDM with FCT and the well-established explicit FDM with FCT for 1D charged particle movements together with the disc method to obtain the electric field in 2D. The streamer

calculations using those FDMs with FCT offer insights into the physics of streamer propagation in terms of electric field and charged particle density evolution over the streamer advancing time.

All the numerical findings of streamer discharge modeling from the implicit streamer model are in agreement with explicit FDM with FCT streamer calculations. The implicit FDM with FCT presented in this work is numerically stable for streamer simulations and allows for larger time steps than the explicit FDM with FCT, making it more computationally efficient despite its higher computational cost per time step. Both implicit and explicit FDM with FCT work well with both adaptive and fixed meshes. However, the implicit FDM provides numerically stable results even when using finer mesh elements around the streamer front in the adaptive mesh than in the explicit FDM, where density gradients and high electric fields are most pronounced.

The electric field is calculated with good accuracy and verified by obtaining the line integral of the electric field. The accuracy of the electric field can be further improved by increasing the sets of image charges considered in the disc method. Photoinization expands the effective ionization region in front of the streamer head along the the streamer axis more than the impact ionization alone, leading to faster streamer propagation.

The total electrons, total charge in the simulation domain, streamer positioning in the air gap and, consequently, the bridging time from both the implicit and explicit FDM streamer models align with the results from existing 2D streamer simulations. Even though the presented streamer calculation has the limitation of assuming a constant radius of the streamer due to the simplicity in numerical implementation, reduced computational time, accuracy in the solution, and the ability of refining theoretical concepts are obtained.

Author Contributions: Conceptualization, H.J., L.A., R.M. and V.C.; methodology, H.J., L.A., R.M. and V.C.; software, H.J.; validation, H.J., L.A., R.M. and V.C.; formal analysis, H.J., L.A. and R.M.; investigation, H.J., L.A., R.M. and V.C.; writing—original draft preparation, H.J.; writing—review and editing, L.A., R.M. and V.C.; visualization, H.J.; supervision, L.A., R.M. and V.C.; funding acquisition, L.A. and V.C. All authors have read and agreed to the published version of the manuscript.

Funding: This research received no external funding.

Institutional Review Board Statement: Not applicable.

Informed Consent Statement: Not applicable.

Data Availability Statement: Data are contained within the article.

Conflicts of Interest: The authors declare no conflicts of interest.

References

1. Nijdam, S.; Teunissen, J.; Ebert, U. The physics of streamer discharge phenomena. *Plasma Sources Sci. Technol.* **2020**, *29*, 103001. [CrossRef]
2. Dijcks, S.; van der Leegte, M.; Nijdam, S. Imaging and reconstruction of positive streamer discharge tree structures. *Plasma Sources Sci. Technol.* **2023**, *32*, 045004. [CrossRef]
3. Cooray, V.; Jayasinghe, H.; Rubinstein, M.; Rachidi, F. The Geometry and Charge of the Streamer Bursts Generated by Lightning Rods under the Influence of High Electric Fields. *Atmosphere* **2022**, *13*, 2028. [CrossRef]
4. Gallimberti, I. The mechanism of the long spark formation. *J. Phys. Colloq.* **1979**, *40*, C7–C193. [CrossRef]
5. Gallimberti, I.; Bacchiega, G.; Bondiou-Clergerie, A.; Lalande, P. Fundamental processes in long air gap discharges. *C. R. Phys.* **2002**, *3*, 1335–1359. [CrossRef]
6. Arevalo, L.; Cooray, V.; Wu, D.; Jacobson, B. A new static calculation of the streamer region for long spark gaps. *J. Electrost.* **2012**, *70*, 15–19. [CrossRef]
7. Ivanovskiy, A. On the mechanisms of lightning initiation and positive leader intergrowth. *Phys. Lett. A* **2022**, *440*, 128112. [CrossRef]

8. Lin, L.; Meng, X.; Mei, H.; Wang, L. Mechanism of Positive Streamer Discharge Under Intense Vertical Component Electric Field. *IEEE Trans. Dielectr. Electr. Insul.* **2025**, *32*, 392–399. [CrossRef]
9. Fang, Y.; Zeng, H.; Yang, B.; Mao, S.; Fang, J. Analysis and comparison of streamer discharge characteristics in equipotential live-line work gap and its simplified gaps under positive switching impulse. *J. Electrost.* **2024**, *132*, 103985. [CrossRef]
10. Zhang, X.; Wang, F.; Liu, N.; Li, A.; Fan, W. Particle simulation of streamer discharges on surface of DC transmission line in presence of raindrops. *J. Appl. Phys.* **2021**, *129*, 183306.
11. Ebert, U.; Montijn, C.; Briels, T.M.P.; Hundsdorfer, W.; Meulenbroek, B.; Rocco, A.; van Veldhuizen, E.M. The multiscale nature of streamers. *Plasma Sources Sci. Technol.* **2006**, *15*, S118. [CrossRef]
12. Teunissen, J.; Ebert, U. Simulating streamer discharges in 3D with the parallel adaptive Afivo framework. *J. Phys. D Appl. Phys.* **2017**, *50*, 474001. [CrossRef]
13. Dawson, G.A.; Winn, W.P. A model for streamer propagation. *Z. Phys.* **1965**, *183*, 159–171. [CrossRef]
14. Gallimberti, I. A computer model for streamer propagation. *J. Phys. D Appl. Phys.* **1972**, *5*, 2179–2189. [CrossRef]
15. Morrow, R.; Lowke, J.J. Streamer propagation in air. *J. Phys. D Appl. Phys.* **1997**, *30*, 614. [CrossRef]
16. Zhuang, C.; Zeng, R. A local discontinuous Galerkin method for 1.5-dimensional streamer discharge simulations. *Appl. Math. Comput.* **2013**, *219*, 9925–9934. [CrossRef]
17. Agnello, R.; Fubiani, G.; Furno, I.; Guittienne, P.; Howling, A.; Jacquier, R.; Taccogna, F. A 1.5D fluid—Monte Carlo model of a hydrogen helicon plasma. *Plasma Phys. Control. Fusion* **2022**, *64*, 055012. [CrossRef]
18. Bagheri, B.; Teunissen, J.; Ebert, U.; Becker, M.M.; Chen, S.; Ducasse, O.; Eichwald, O.; Loffhagen, D.; Luque, A.; Mihailova, D.; et al. Comparison of six simulation codes for positive streamers in air. *Plasma Sources Sci. Technol.* **2018**, *27*, 095002. [CrossRef]
19. Wang, Z.; Sun, A.; Teunissen, J. A comparison of particle and fluid models for positive streamer discharges in air. *Plasma Sources Sci. Technol.* **2022**, *31*, 015012. [CrossRef]
20. Aleksandrov, N.L.; Bazelyan, E.M. Simulation of long-streamer propagation in air at atmospheric pressure. *J. Phys. D Appl. Phys.* **1996**, *29*, 740. [CrossRef]
21. Morrow, R.; Blackburn, T.R. The stepped nature of lightning, and the upward connecting streamer. *J. Phys. D Appl. Phys.* **2002**, *35*, L69. [CrossRef]
22. Strobel, L.R.; Guerra-Garcia, C. Numerical investigation of the bridging and current flow of a positive DC streamer using a 1.5D model. *J. Phys. D Appl. Phys.* **2025**, *58*, 105203. [CrossRef]
23. Bessières, D.; Paillol, J.; Bourdon, A.; Ségur, P.; Marode, E. A new one-dimensional moving mesh method applied to the simulation of streamer discharges. *J. Phys. D Appl. Phys.* **2007**, *40*, 6559. [CrossRef]
24. Wang, L.; Bao, H.; Ding, D.; Chen, R. Numerical Simulation of Streamer Discharge Modeled by Drift-Diffusion Equations Based on SETD Method. *IEEE Trans. Plasma Sci.* **2022**, *50*, 525–533. [CrossRef]
25. Georghiou, G.E.; Morrow, R.; Metaxas, A.C. The theory of short-gap breakdown of needle point-plane gaps in air using finite-difference and finite-element methods. *J. Phys. D Appl. Phys.* **1999**, *32*, 1370. [CrossRef]
26. Hui, J.; Guan, Z.; Wang, L.; Li, Q. Variation of the Dynamics of Positive Streamer with Pressure and Humidity in Air. *IEEE Trans. Dielectr. Electr. Insul.* **2008**, *15*, 382–389. [CrossRef]
27. Bian, X.; Zhu, J.; Yang, W.; Wan, S.; Qi, L.; Li, X.; Li, H. The role of low air pressure in the variation of negative corona-generated space charge in a rod to plane electrode. *High Volt.* **2018**, *3*, 126–132.
28. Aleksandrov, N.L.; Bazelyan, E.M. Temperature and density effects on the properties of a long positive streamer in air. *J. Phys. D Appl. Phys.* **1996**, *29*, 2873. [CrossRef]
29. Aleksandrov, N.L.; Bazelyan, M.; Novitskii, D.A. Influence of moisture on the properties of long streamers in air. *Tech. Phys. Lett.* **1998**, *24*, 367–368. [CrossRef]
30. Zalesak, S.T. Fully multidimensional flux-corrected transport algorithms for fluids. *J. Comput. Phys.* **1979**, *31*, 335–362. [CrossRef]
31. Steinle, P.; Morrow, R. An implicit flux-corrected transport algorithm. *J. Comput. Phys.* **1989**, *80*, 61–71. [CrossRef]
32. Morrow, R. An Implicit Flux-Corrected Transport Algorithm Used for Gas Discharge Calculations. *Plasma* **2025**, *8*, 7. [CrossRef]
33. Komuro, A.; Yoshino, A.; Wei, Z.; Ono, R. Effects of oxygen concentration on streamer propagation and ozone production in a single-filament streamer discharge at atmospheric pressure. *J. Phys. D Appl. Phys.* **2023**, *56*, 185201. [CrossRef]
34. Baohong, G. Simulating Positive and Negative Streamer Discharges in Air and in Strongly Attaching Gases. Ph.D. Thesis, Research TU/e/Graduation TU/e, Eindhoven University of Technology, Eindhoven, The Netherlands, 2023. Available online: https://research.tue.nl/files/312984148/20231207_Guo_hf.pdf (accessed on 18 May 2025).
35. Morrow, R. Theory of electrical corona in SF6. *Nucl. Instruments Methods Phys. Res. Sect. A Accel. Spectrometers Detect. Assoc. Equip.* **1996**, *382*, 57–65.
36. Davies, A. Computation of ionisation growth at high current densities. *Proc. Inst. Electr. Eng.* **1975**, *122*, 765–768. [CrossRef]
37. Jayasinghe, H.; Arevalo, L.; Morrow, R.; Cooray, V. Reduced order model for a streamer discharge in air. In Proceedings of the 37th International Conference on Lightning Protection, Dresden, Germany, 1–7 September 2024; p. 870.

38. Book, D.L.; Boris, J.P.; Hain, K. Flux-corrected transport II: Generalizations of the method. *J. Comput. Phys.* **1975**, *18*, 248–283. [CrossRef]
39. Morrow, R.; Cram, L. Flux-corrected transport and diffusion on a non-uniform mesh. *J. Comput. Phys.* **1985**, *57*, 129–136. [CrossRef]
40. Morrow, R. Numerical solution of hyperbolic equations for electron drift in strongly non-uniform electric fields. *J. Comput. Phys.* **1981**, *43*, 1–15. [CrossRef]
41. Penney, G.W.; Hummert, G.T. Photoionization Measurements in Air, Oxygen, and Nitrogen. *J. Appl. Phys.* **1970**, *41*, 572–577. [CrossRef]
42. Morrow, R. Theory of Positive Corona in SF6 Due to a Voltage Impulse. *IEEE Trans. Plasma Sci.* **1991**, *19*, 86–94. [CrossRef]
43. Morrow, R. Space-charge effects in high-density plasmas. *J. Comput. Phys.* **1982**, *46*, 454–461. [CrossRef]
44. Morrow, R. Numerical modelling of time-dependent electrical breakdown in non-uniform electric fields. In Proceedings of the 18th International Conference on Phenomena in Ionised Gases, Swansea, UK, 13–17 July 1987; p. 268.
45. Kulikovsky, A.A. The role of photoionization in positive streamer dynamics. *J. Phys. D Appl. Phys.* **2000**, *33*, 1514. [CrossRef]
46. Naidis, G.V. Effects of photoionization characteristics on parameters of positive streamers. *Plasma Res. Express* **2018**, *1*, 017001. [CrossRef]
47. Wei, Z.; Komuro, A.; Ono, R. The influence of individual evaluation of electron-impact ionization, attachment, and photoionization rates on positive streamer propagation. *Plasma Processes Polym.* **2024**, *21*, 2300113,
48. Starikovskiy, A.Y.; Aleksandrov, N.L. How pulse polarity and photoionization control streamer discharge development in long air gaps. *Plasma Sources Sci. Technol.* **2020**, *29*, 075004. [CrossRef]
49. Pavan, C.; Martinez-Sanchez, M.; Guerra-Garcia, C. Investigations of positive streamers as quasi-steady structures using reduced order models. *Plasma Sources Sci. Technol.* **2020**, *29*, 095004. [CrossRef]

Disclaimer/Publisher's Note: The statements, opinions and data contained in all publications are solely those of the individual author(s) and contributor(s) and not of MDPI and/or the editor(s). MDPI and/or the editor(s) disclaim responsibility for any injury to people or property resulting from any ideas, methods, instructions or products referred to in the content.